

High-Resolution Near-Infrared Polarimetry of a Circumstellar Disk around UX Tau A

Ryoko TANI¹, Yoichi ITOH¹, Tomoyuki KUDO², Tomonori HIOKI¹, Yumiko OASA³, Ranjan GUPTA⁴, A. K. SEN⁵, J. P. WISNIEWSKI⁶, T. MUTO²⁵, C. A. GRADY^{9,10,11}, J. HASHIMOTO¹², M. FUKAGAWA¹³, S. MAYAMA¹⁴, J. HORNBECK¹⁵, M. SITKO^{16,17,18}, R. RUSSELL^{18,19}, C. WERREN^{17,18}, M. CURÉ²⁰, T. CURRIE¹⁰, N. OHASHI^{2,21}, Y. OKAMOTO²², M. MOMOSE²², M. HONDA²³, S. -I. INUTSUKA²⁴, T. TAKEUCHI²⁵, R. DONG²⁶, L. ABE²⁷, W. BRANDNER²⁸, T. BRANDT²⁶, J. CARSON²⁹, S. EGNER², M. FELDT²⁸, T. FUKUE¹², M. GOTO²⁸, O. GUYON², Y. HAYANO², M. HAYASHI³⁰, S. S. HAYASHI², T. HENNING²⁸, K. W. HODAPP³¹, M. ISHII², M. IYE¹², M. JANSON²⁶, R. KANDORI¹², G. P. KNAPP²⁶, N. KUSAKABE¹², M. KUZUHARA^{12,30}, T. MATSUO³², M. W. McELWAIN²⁶, S. MIYAMA¹², J. -I. MORINO¹², A. MORO-MARTÍN³³, T. NISHIMURA², T. -S. PYO², G. SERABYN⁸, H. SUTO¹², R. SUZUKI¹², M. TAKAMI²¹, N. TAKATO², H. TERADA², C. THALMANN²⁸, D. TOMONO², E. L. TURNER^{7,26}, M. WATANABE³⁴, T. YAMADA³⁵, H. TAKAMI², T. USUDA², and M. TAMURA¹²

¹*Graduate School of Science, Kobe University, 1-1 Rokkodai-cho, Nada-ku, Kobe, Hyogo 657-8501
tanii@stu.kobe-u.ac.jp*

²*Subaru Telescope, National Astronomical Observatory of Japan, 650 North A'ohoku Place, Hilo, HI 96720, USA*

³*Faculty of Education, Saitama University, 255 Shimoookubo, Sakura, Saitama, Saitama 338-0825*

⁴*Inter University Center for Astronomy and Astrophysics(IUCAA), Ganeshkhind, Pune 411 007, India*

⁵*Department of Physics, Assam University, Silchar 788011, Assam, India*

⁶*Department of Astronomy, University of Washington, Box 351580 Seattle, WA 98195, USA*

⁷*Institute for the Physics and Mathematics of the Universe, The University of Tokyo, Kashiwa 227-8568, Japan*

⁸*Jet Propulsion Laboratory, California Institute of Technology, Pasadena, CA, USA*

⁹*Eureka Scientific, 2452 Delmer, Suite 100, Oakland CA 96002, USA*

¹⁰*ExoPlanets and Stellar Astrophysics Laboratory, Code 667, Goddard Space Flight Center, Greenbelt, MD 20771 USA*

¹¹*Goddard Center for Astrobiology*

¹²*National Astronomical Observatory of Japan, 2-21-1 Osawa, Mitaka, Tokyo 181-8588, Japan*

¹³*Department of Earth and Space Science, Graduate School of Science, Osaka University, 1-1, Machikaneyama, Toyonaka, Osaka 560-0043, Japan*

¹⁴*The Graduate University for Advanced Studies (SOKENDAI), Shonan International Village, Hayama-cho, Miura-gun, Kanagawa, 240-0193, Japan*

- ¹⁵*Department of Physics and Astronomy, University of Louisville, Louisville, KY 40292, USA*
- ¹⁶*Space Science Institute, 4750 Walnut St., Suite 205, Boulder, CO 80301, USA*
- ¹⁷*Department of Physics, University of Cincinnati, Cincinnati, OH 45221-0011, USA*
- ¹⁸*Visiting Astronomer, NASA Infrared Telescope Facility, operated by the University of Hawaii
under contract to NASA*
- ¹⁹*The Aerospace Corporation, Los Angeles, CA 90009, USA*
- ²⁰*Departamento de Física y Astronomía, Facultad de Ciencias, Universidad de Valparaíso Av. Gran
Bretaña 1111, Casilla 5030, Valparaíso, Chile*
- ²¹*Institute of Astronomy and Astrophysics, Academia Sinica, P.O. Box 23-141, Taipei 106, Taiwan*
- ²²*Faculty of Science, Ibaraki University, 2-1-1 Bunkyo, Mito, Ibaraki, 310-8512, Japan*
- ²³*Department of Information Science, Kanagawa University, 2946 Tsuchiya, Hiratsuka, Kanagawa
259-1293, Japan*
- ²⁴*Department of Physics, Nagoya University, Furo-cho, Chikusa-ku, Nagoya, Aichi, 464-8602, Japan*
- ²⁵*Tokyo Institute of Technology, 2-12-1 Ookayama, Meguro, Tokyo 152-8551, Japan*
- ²⁶*Department of Astrophysical Sciences, Princeton University, NJ08544, USA*
- ²⁷*Laboratoire Hippolyte Fizeau, UMR6525, Universite de Nice Sophia-Antipolis, 28, avenue Valrose,
06108 Nice Cedex 02, France*
- ²⁸*Max Planck Institute for Astronomy, Heidelberg, Germany*
- ²⁹*Department of Physics and Astronomy, College of Charleston, 58 Coming St., Charleston, SC
29424, USA*
- ³⁰*Department of Astronomy, The University of Tokyo, Hongo 7-3-1, Bunkyo-ku, Tokyo 113-0033,
Japan*
- ³¹*Institute for Astronomy, University of Hawaii, 640 North A'ohoku Place, Hilo, HI 96720, USA*
- ³²*Department of Astronomy, Kyoto University, Kitashirakawa-Oiwake-cho, Sakyo-ku, Kyoto,
606-8502, Japan*
- ³³*Department of Astrophysics, Center for Astrobiology, Ctra. de Ajalvir, km 4, Torrejón de Ardoz,
28850, Madrid, Spain*
- ³⁴*Department of CosmoSciences, Hokkaido University, Sapporo, 060-0810, Japan*
- ³⁵*Astronomical Institute, Tohoku University, Aoba, Sendai, 980-8578, Japan*

(Received ; accepted)

Abstract

We present *H*-band polarimetric imagery of UX Tau A taken with HiCIAO/AO188 on the Subaru Telescope. UX Tau A has been classified as a pre-transitional disk object, with a gap structure separating its inner and outer disks. Our imagery taken with the 0.15'' (21 AU) radius coronagraphic mask has revealed a strongly polarized circumstellar disk surrounding UX Tau A which extends to 120 AU, at a spatial resolution of 0.1'' (14 AU). It is inclined by $46^\circ \pm 2^\circ$ as the west side is nearest.

Although SED modeling and sub-millimeter imagery suggested the presence of a gap in the disk, with the inner edge of the outer disk estimated to be located at 25 – 30 AU, we detect no evidence of a gap at the limit of our inner working angle (23AU) at the near-infrared wavelength. We attribute the observed strong polarization (up to 66 %) to light scattering by dust grains in the disk. However, neither polarization models of the circumstellar disk based on Rayleigh scattering nor Mie scattering approximations were consistent with the observed azimuthal profile of the polarization degrees of the disk. Instead, a geometric optics model of the disk with nonspherical grains with the radii of 30 μm is consistent with the observed profile. We suggest that the dust grains have experienced frequent collisional coagulations and have grown in the circumstellar disk of UX Tau A.

Key words: (stars:) planetary systems: protoplanetary disk – techniques: high angular resolution – techniques: polarimetric

1. Introduction

A protoplanetary disk around a young stellar object is the site of planetary formation. The core accretion model (e.g., Nakagawa et al. 1983) and the gravitational instability model (e.g., Boss 1998) are two possible methods by which the process of planet formation might occur. In the core accretion model, a key process is dust grain growth by collisional coagulations. Several fundamental processes of the dust growth have been proposed under simple assumptions. Dust grains with sizes less than a few tens of micrometers orbit a central star with the same velocity as gas (Adachi et al. 1976). They frequently collide and coagulate with each other. Simultaneously they begin to settle into an equatorial plane of the disk (Nakagawa et al. 1981). Dust grains with different settling velocities also experience collisional coagulations. As a result, planetesimals (radii $\sim 10 - 100$ km; Kokubo & Ida 1998) are formed in the mid-plane of the disk. Bodies between a few tens of micrometers and a few kilometers are dominated by gas drag. Such bodies are thought to migrate towards the central star in a short timescale (e.g., Nakagawa et al. 1986). This rapid inward migration poses a challenge to planet formation theory. By contrast, for planetesimals larger than a few kilometers, gravitational interactions are significant and relative velocities between the bodies increase due to mutual perturbations. This situation allows faster growth of the larger bodies and leads to formation of planetary embryos (radii ~ 1000 km; Kokubo & Ida 2000). The core accretion model is one of the plausible model of planetary formation. However it is still debated how sub-micron sized grains are transformed into kilometer sized bodies.

An infrared excess in the spectral energy distribution of a young stellar object provides indirect evidence for the presence of a circumstellar disk. The spectral energy distributions

of T Tauri stars with continuous, optically thick disks have strong infrared excesses in the near-infrared to far-infrared wavelengths (Williams & Cieza 2011). Recently, objects with large continuum excesses in the mid- to far-infrared wavelengths but no excess in the near-infrared wavelengths have been discovered, called 'transitional disk objects' (TDOs; Calvet et al. 2002, Calvet et al. 2005). Such an object is considered to lie in the transition state between classical T Tauri stars (CTTSs) and weak-line T Tauri stars (WTTSSs). It is expected that the inside of the disk has been cleared out by dust accumulations and/or formations of protoplanets. Photo-evaporation process is also proposed as a mechanism to create a transitional disk. On the other hand, 'pre-transitional disk objects' (PTDOs) are considered to be in the evolutionary phase before reaching the transitional disk phase. They have mid- to far-infrared excesses similar to TDOs, however, they also show small excess in the near-infrared wavelengths (Espaillat et al. 2007). The slight near-infrared excess implies that optically thick material remains in the innermost part of the disk. Espaillat et al. (2010) proposed that the planetary formation process is expected to progress in the gap structures between the inner and outer disks.

High spatial resolution coronagraphic imaging polarimetry is one way to directly diagnose young circumstellar disks. The degree of polarization depends on scattering angle, grain size, and composition. By constructing the polarization profile of the disk, we are able to investigate size and composition of dust grains. Silber et al. (2000) conducted infrared polarization imaging observations of a circumbinary disk around GG Tau with NICMOS mounted on the Hubble Space Telescope. The circumbinary disk shows strong polarization degrees of $\sim 50\%$ at $1 \mu\text{m}$ wavelength. The polarization azimuthal profile indicated Rayleigh-like scattering from dust grains with sub-micron size. Hashimoto et al. (2011) conducted H -band polarization imaging observations of AB Aur with HiCIAO/AO188 on the Subaru Telescope and revealed spiral structure in the outer part and the double ring structure at the inner part of the circumstellar disk. There was a number of studies in the last years, using the same observational technique for similar sources, e.g., Apai et al. (2004; TW Hya), Oppenheimer et al. (2008; AB Aur), Perrin et al. (2009; AB Aur), Quanz et al. (2011; HD100546), Quanz et al. (2012; HD97048).

UX Tau is a T Tauri multiple system (Jones & Herbig 1979) in the Taurus molecular cloud (distance ~ 140 pc; Elias 1978). It consists of a primary star (UX Tau A), with UX Tau B separated by $5.86''$ and UX Tau C separated by $2.63''$ from the primary. UX Tau B is itself a binary system with the separation of $0.14''$. The spectral type of UX Tau A is K2 (Kraus & Hillenbrand 2009). Its spectral energy distribution shows a slight excess in the near-infrared wavelengths and significant excesses in the mid- and far-infrared wavelengths. These characteristics indicate that UX Tau A has an optically thick inner disk separated from an optically thick outer disk by a gap, i.e. it is a pre-transitional disk object (Espaillat et al. 2010). Model fits of the SED suggested that the outer edge of the inner disk is located at < 0.21 AU and the inner wall of the outer disk is located at 30 AU from the central star (Espaillat et al. 2010, 2011). The disk around UX Tau A was spatially resolved by Sub-millimeter Array

at $880 \mu\text{m}$ wavelength, with the spatial resolution of $0.3''$ (Andrews et al. 2011). They found a dust-depleted disk cavity around the central star, and estimated the inner edge of the outer disk to be located 25 AU from the central star. UX Tau A shows no $10 \mu\text{m}$ silicate emission (Espaillat et al. 2010), implying a lack of small dust grains in the disk. These features suggest dust grain growth in the circumstellar disk of UX Tau A. We conducted polarization imaging observations of UX Tau A in the H -band ($1.6 \mu\text{m}$) and investigate the collisional coalescence process of the dust grains in its disk.

2. Observations

Near-infrared (H -band; $1.6 \mu\text{m}$) polarimetric imaging observations of UX Tau A were carried out 2009 December 23 with HiCIAO (High Contrast Instrument for the Subaru next generation Adaptive Optics; Tamura et al. 2006) and the adaptive optics system, AO188 (Hayano et al. 2010), mounted on the Nasmyth platform of the Subaru Telescope (Table 1). These observations were conducted as part of the larger SEEDS survey (Tamura 2009). We employed the Polarization Differential Imaging (PDI) mode. The Wollaston prism installed in HiCIAO divides incident light into two linearly polarized components which are perpendicular to each other and which are imaged simultaneously on the detector. Each image has 1024×2048 pixels with a field of view of $9.75'' \times 20.09''$ and pixel scale of 9.521 mas/pixel in the east-west direction and 9.811 mas/pixel in the north-south direction. In the PDI mode, when the half-wave plate is set at the offset angle of 0° , 45° , 22.5° , and 67.5° , we obtain polarimetric images with the polarization direction at 0° and 90° , 90° and 0° , 45° and 135° , and 135° and 45° components respectively. We used a coronagraphic mask with $0.3''$ diameter to suppress the brightness of UX Tau A. We obtained 44 frames, i.e. 11 frames per half-wave plate position, of UX Tau A with an exposure time of 60 s. The outside of the coronagraphic mask was not saturated. During the observations we fixed the star at the center of the coronagraphic mask, i.e. dithering method was not employed. In these frames, the tertiary component (UX Tau C) was also imaged outside the coronagraphic mask. The PSF reference star SAO93770 was imaged before observing UX Tau, using the PDI mode with the $0.3''$ diameter coronagraphic mask. The natural seeing was $0.5 - 0.6''$ in the K -band. The AO188 measures the wavefront distortion by the atmospheric turbulence in the R -band wavelength and compensates it at all wavelength. The FWHM of UX Tau C was 10 pixels ($\sim 0.1''$) on average. In the observations of SAO93770, with the ND filter in the AO device, we set the brightness difference between it and UX Tau to be 0.07 mag in the R -band in order to level the AO correction performance in the observations of the object and the reference star. We took 11 frames with an exposure time of 90 s without employing dithering method. We obtained 10 flat frames on the same day as the target observations and 49 dark frames in 2009 December 24. Each exposure time was 80 s for the flat frames and 5.6 s for the dark frames. The dark frames were used only for the identification of hot pixels.

Table 1. Properties of the observing objects

Target	RA [J2000]	DEC [J2000]	Sp.Type*	H [mag]**	Airmass
UX Tau A	04 30 03.991	+18 13 49.39	K2	8.0	1.2 – 1.6
UX Tau C	04 30 03.991	+18 13 49.39	M5	10.9	1.2 – 1.6
SAO93770	04 07 08.734	+10 47 58.86	F8	7.0	1.2 – 1.3

* Kraus & Hillenbrand (2009) for UX Tau A and C. The Hipparcos and Tycho Catalogues for SAO93770. ** Correia et al. (2006) for UX Tau A and C. NOMAD catalog for SAO93770.

3. Data Reduction

The object frames were calibrated with the Image Reduction and Analysis Facility (IRAF). All frames of HiCIAO/AO188 have artifacts of horizontal stripes and vertical bandings. The horizontal stripe has a size of 2048×64 pixels. Each frame has 32 horizontal stripes. We attribute the origin of these artifacts to a bias instability caused by temperature fluctuations between the detector and the Application Specific Integrated Circuit (ASIC). The ASIC translates the detector’s analog signals into the digital signals. The vertical bandings occur at one pixel interval. They show an alternate direction between even and odd horizontal stripes.

To mitigate these artifacts, first, the horizontal stripes were removed from the dark frames. We measured a median count for each horizontal stripe and subtracted it from each horizontal stripe. For the vertical bandings, even horizontal stripes were vertically flipped. We median-combined 32 horizontal stripes to make a master horizontal stripe. We subtracted the master stripe from each odd horizontal stripe. From each even horizontal stripe, the vertically flipped master stripe was subtracted. Finally, the dark frames were median-combined. This combined dark frame was only used as a mask frame for the extraction of hot pixels.

Next, we eliminated hot and bad pixels from the object and flat frames. We regarded the pixels with more than 100 ADU in the combined dark frame as hot pixels. It is nearly equivalent to 12σ above the median of the combined dark frame. Hot pixels were replaced with 10000 ADU and the other pixels were replaced with 0 ADU. Using this frame as a hot pixel mask, hot pixels were interpolated by nearest good pixels in the object and flat frames. Then, we removed the stripe patterns from the object frames with the same procedure we used for the dark frames. In this process, however, we put circular masks on the stars and computed the median values of the stripes and the bandings except the mask regions. We considered that dark counts were also subtracted from the object frames through this destriping process. We did not subtract the stripes from the flat frames. Because the flat frames had counts two orders of magnitude larger than the stripes, we ignored the stripe modulations. The flat frames were median-combined and normalized to 1 ADU. The object frames were divided by the flat frame. Bad pixels and cosmic rays were interpolated by nearest good pixels in the object frames.

After those processes, we obtained the flux images of the polarimetric components, F_{0°

and F_{90° , F_{90° and F_{0° , F_{45° and F_{135° , and F_{135° and F_{45° , separated into left and right of the image by ~ 1070 pixels with each other. We cut the object frames into the left and right images. Each image has a $9.75'' \times 20.09''$ field of view. For each image, distortions caused by the Wollaston prism was corrected. Then, the central coordinates of the companion, UX Tau C, in all object images were measured. Using those coordinates, the object images were aligned. We also carried out the same procedures for the PSF reference star frames. The position of the photo-center of the reference star was estimated by fitting the halo component with a 2D Gaussian profile. Two frames of UX Tau A and three frames of the PSF reference star were not included in the following process, since they had insufficient tip-tilt correction.

Linear polarization is described by the degree of polarization P and polarization angle α . These values are derived with the Stokes parameters, I , Q , and U

$$\frac{Q}{I} = \frac{F_{0^\circ} - F_{90^\circ}}{F_{0^\circ} + F_{90^\circ}} \quad (1)$$

$$\frac{U}{I} = \frac{F_{45^\circ} - F_{135^\circ}}{F_{45^\circ} + F_{135^\circ}} \quad (2)$$

$$P = \sqrt{\left(\frac{Q}{I}\right)^2 + \left(\frac{U}{I}\right)^2} \quad (3)$$

$$\alpha = \frac{1}{2} \arctan\left(\frac{U}{Q}\right), \quad (4)$$

where F_{0° , F_{90° , F_{45° , and F_{135° are the intensity of each polarimetric component. By subtracting the right images from the left images, we derived 11 images of Q and $-Q$, and 10 images of U and $-U$. This subtraction method suppressed speckle noises that appeared both in the right and left images. We subtracted the $-Q$ images from the Q images and the $-U$ from the U . Thus, different aberrations between the left and right images due to the different dividing directions of the Wollaston prism were cancelled (double-difference technique; Hinkley et al. 2009). $2Q$ and $2U$ images were divided by 2, then the Q and U images were combined respectively. Then, we corrected the instrumental polarization induced from the telescope and the instruments. We refer to Joos et al. (2008) for the correction. First, we construct a 2×2 Jones matrix for each optical element. In the HiCIAO case, we consider that the tertiary mirror and three mirrors of the derotator are probably dominant sources of the instrumental polarization. The surface materials of the mirrors expressed by the complex reflection index ($n = \eta + i\kappa$) was actually measured by the ellipsometer. We also describe the rotation of Stokes vectors as a function of the parallactic angle. Then, the multiplication of all single Jones matrices leads to a Jones matrix of whole telescope/instrument for a given set-up. Finally, the constructed Jones matrix was inverted and multiplied with the measured Stokes vectors to obtain the original Stokes vectors on the sky. In above method, we assumed monochromatic light and infinite F-number.

These images had distortions by the compensator in HiCIAO, the AO system, and the telescope. The compensator is located in front of the focal mask and reduces chromatic aberrations. By using images of M15 observed by the HST and HiCIAO, we calibrated the image distortion of Q and U . Multiplying both sides of equation (3) by I , we obtain the following equation,

$$PI = \sqrt{Q^2 + U^2}. \quad (5)$$

We constructed polarized intensity (PI) images with the Q and U images. Assuming that polarization due to the interstellar materials in front of UX Tau is negligible (See Section 4), the polarized intensity image represents the polarized component of circumstellar structures around the central star.

In order to derive the polarization P of the circumstellar structures, the PI image needs to be divided by the I image which contains only the components of the circumstellar structures. The I image of UX Tau A (hereafter I_{tot}) consists of the intensity of the circumstellar structures as well as that of the central star. By subtracting the I component of the central star (hereafter I_*) from the I_{tot} , we obtain the I image of the circumstellar structures (hereafter I_{disk}), i.e. $I_{\text{disk}} = I_{\text{tot}} - I_*$. We adopted the I image of the PSF reference star (hereafter I_{psf}) as the I_* . First, we constructed I images. We used the left and right images, F_{0° and F_{90° , F_{90° and F_{0° , F_{45° and F_{135° , and F_{135° and F_{45° . For UX Tau, we combined the left and right images into I_{tot} images. For the PSF reference star, the central star position was measured in each image with fitting the halo component with a 2D Gaussian profile, then the position offset was corrected. Then we combined the left and right images into the I_{psf} image. The image distortion was also calibrated. Two frames of the PSF reference star have distorted PSFs, so that we used six frames of the PSF reference star in the following procedure.

Since the Subaru Telescope is an alt-azimuth telescope and HiCIAO is mounted on the Nasmyth platform, the position angle of the spider changes in each image. The I_{psf} images were rotated to adjust their spider directions to those of every I_{tot} image. The six I_{psf} images of the PSF reference star were median-combined to make a PSF template I image (hereafter $I_{*\text{tmp}}$) for each I_{tot} image. Finally, we made 42 $I_{*\text{tmp}}$ images. From these I_{tot} and $I_{*\text{tmp}}$ images, sky levels were subtracted. The sky value was the average of the mean counts of four regions. The regions were selected as the 100×100 pixel regions separated at least $5''$ from the central star. Next, we made the I_{disk} image. In each I_{tot} and $I_{*\text{tmp}}$ image, we measured halo intensities of the central star. The evaluated regions were four regions of 20×20 pixels, which had a distance of 150 pixel ($1.47''$) from the central star and did not overlap the spider directions. We used the ratio of the mean values of these halos to determine the proper scaling to apply to $I_{*\text{tmp}}$ image during PSF subtraction. We also shifted $I_{*\text{tmp}}$ image slightly so that intensity of the circumstellar disk would not show strong asymmetry in the residual image. We assume that the disk intensity is symmetric, thus we may have over-corrected the PSF subtraction.

The amount of the shift was 1.3 pixels ($0.01'' = 0.1 \text{ FWHM} \sim 2 \text{ AU}$) on average. Therefore, the inner working angle of the I_{disk} image is $\sim 23 \text{ AU}$. Then, we subtracted $I_{*\text{tmp}}$ image from I_{tot} image. This process was performed in each I_{tot} image. As a result, we obtained 42 I_{disk} images containing only the circumstellar structure. They were median-combined. Finally, the PI image was divided by the I_{disk} image, thus the P image of the circumstellar structure was generated.

4. Results

We detected strongly polarized components around UX Tau A. The polarized intensity (PI) image shows an elliptical structure (Figure 1). We evaluate the extent of the region where the intensity is more than five times the standard deviation in the sky region of the PI image. It has a semi-major axis of $\sim 0.83''$ ($\sim 120\text{AU}$) with the position angle of $165^\circ \pm 2^\circ$ and a semi-minor axis of $0.58''$ ($\sim 80\text{AU}$).

We associate this polarization structure to the circumstellar disk of UX Tau A. If the circumstellar disk of UX Tau A has a circular and geometrically thin structure, the disk is tilted to east-west with the inclination of $46^\circ \pm 2^\circ$. The west side of the structure is brighter than the east side. We assume that the west side of the structure is the near side to us. We measured degrees and angles of polarization in every 9×9 pixel region. The degree of polarization in regions with $\text{SNR} > 5\sigma$ ranges from 1.6 to 66 %. The polarization vectors show a mostly centrosymmetric pattern centered on UX Tau A, supporting our claim that this structure is attributable to its circumstellar disk. The radial profiles of the polarized intensity along the semi-major axes are shown in Figure 2. The polarized intensity declines with the third power of the disk radius.

Figure 3 shows an azimuthal profile of the polarization degree (P) along the ellipse of $e = 0.72$ ($i = 46^\circ$) and a semi-major axis of $0.30''$ (42 AU). We measured mean polarization degrees and standard deviations in every 9×9 pixel region. It is sinusoidal; two maxima and two minima appear with 90° intervals. This pattern is prominent up to the semi-major axis of $\sim 0.5''$. Figure 4 represents radial profiles of the polarization degree along the semi-major axes. We measured mean polarization degrees and standard deviations in every 9×9 pixel region. The degree of polarization declines with radial distance to $\sim 0.5''$. Beyond $0.8''$ from the central star, the polarization is not significantly detected. Assuming that the polarized intensity and the polarization degree of the disk are constant within binned 9×9 pixels respectively, these uncertainties are up to $\sim 80 \text{ ADU}$ and $\sim 20 \%$ as shown in Figures 2 and 3. These estimates do not take into account any systematic effects from the data reduction such as the PSF subtraction and the correction for the instrumental polarization. Further discussion on the instrumentation and the systematic errors will be presented elsewhere.

Polarization due to interstellar medium in front of UX Tau binary system is negligible. The system is slightly embedded in a molecular cloud; the interstellar extinction of UX Tau A

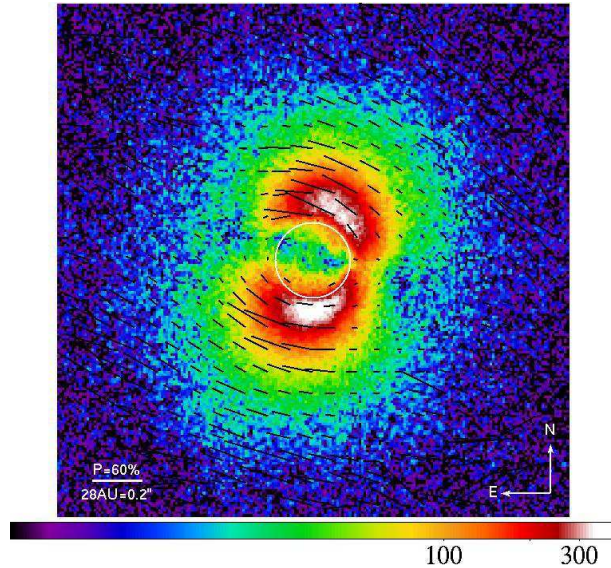


Fig. 1. A polarized intensity image of UX Tau A. The polarization vectors are superimposed in the region where the polarized intensity is larger than 5σ . The vector lengths and directions indicate the degree and angle of the polarization, respectively. The vector scale is shown in the bottom-left. A circle shows the $0.3''$ diameter coronagraphic mask positioned on the central star. The bottom color-bar denotes the polarized intensity in ADU.

is 1.8 mag in the V -band (Espaillat et al. 2010). Serkowski et al. (1975) obtained a relationship between polarization and reddening as $E(B - V) \geq P/9$. We would therefore anticipate little foreground interstellar polarization would be present. Indeed, the polarization degree of UX Tau C, which was measured in 50×50 pixels centered on the star, is only 0.5 %. We do not detect any circumstellar structures around UX Tau C. Since no $880 \mu\text{m}$ emission is detected from UX Tau C (Andrews et al. 2011), this source is unlikely to have circumstellar structures and its measured polarization can be assumed to be a reasonable proxy for the interstellar polarization along the line of sight to UX Tau A. Therefore, the interstellar medium in front of the UX Tau system has only negligible polarization.

Outflows emanating to the north-west and south-east directions are also possible sources to explain the elliptical structure. Lucas et al. (2004) detected the polarization structure around HL Tau and suggested that its strong polarization structure is caused by bipolar outflows. However, the disk around UX Tau A has already been imaged by Sub-millimeter Array (Andrews et al. 2011). The inclination and the position angle of the semi-major axis of the disk were determined to be 35° and 176° , respectively. The disk geometry is roughly consistent with that derived from the polarized intensity image. Therefore, we consider that the elliptical structure we detected is not attributed to the outflow, but to the circumstellar disk around the central star.

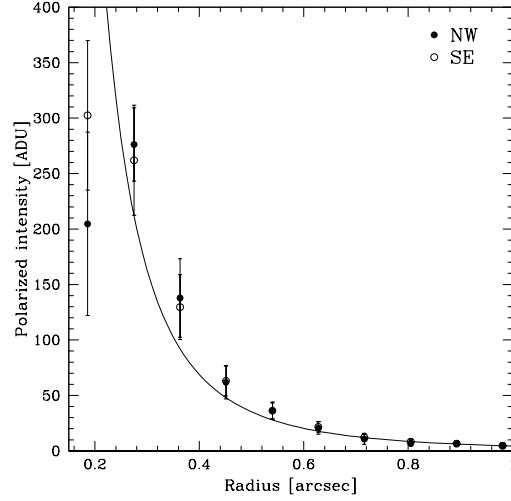


Fig. 2. Radial profiles of the polarized intensity measured along semi-major axes of the circumstellar disk of UX Tau A. The plots and the errorbars show mean polarized intensity and standard deviation in every 9×9 pixel region. The filled and open circles denote the polarization intensity along semi-major axes in the north-west and south-east directions, respectively. The solid line show a power law fitting to the observed radial profile. The polarized intensity declines as the third power of the disk radius.

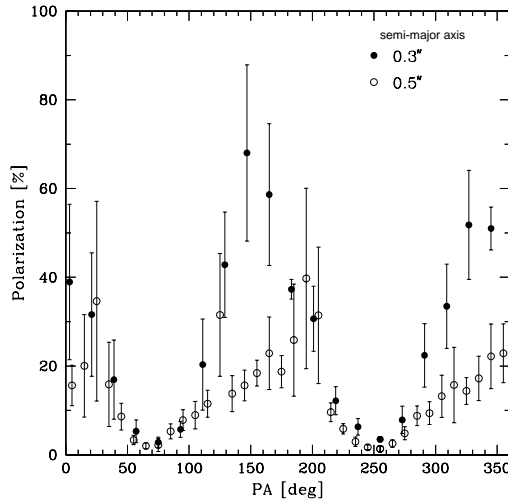


Fig. 3. An azimuthal profile of the polarization degree of the circumstellar disk. It is measured on the ellipse of eccentricity $e = 0.72$ and a semi-major axis of $0.30''$ and $0.50''$, which corresponds to the disk radius of ~ 40 AU and 70 AU. For the position angle (PA), north is 0° and east is 90° . The plots show mean polarization degrees binned in 9×9 pixels, and maxima and minima are clearly seen in 90° intervals.

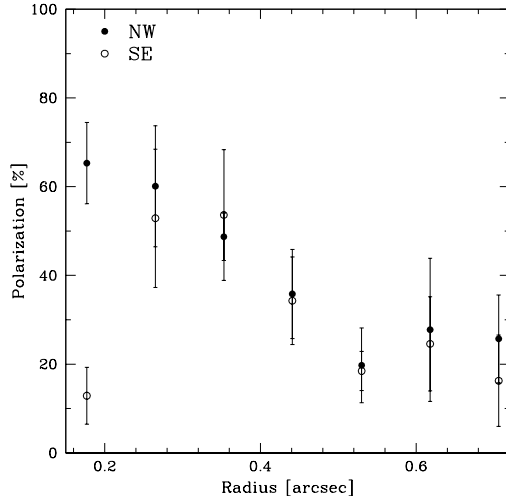


Fig. 4. Radial profiles of the polarization degrees measured along semi-major axes of the circumstellar disk of UX Tau A. The plots show mean polarization degrees binned in 9×9 pixels. The filled and open circles denote the polarization degrees along semi-major axes in the north-west and south-east directions, respectively. From $0.15''$ to $0.50''$, the degrees of polarization show decreasing trends.

5. Discussion

5.1. Geometry of the circumstellar disk

The circumstellar disk looks smooth. A gap-like structure at $0.21 - 30$ AU is suggested from the disk model fitting to the SED (Espaillat et al. 2010, 2011). A disk cavity is also resolved by the SMA observations (Andrews et al. 2011), which is identical with the outer radius of the gap structure. However, we do not find such a structure. Our data do not show any signs for a gap or cavity down to the achieved inner working angle (~ 23 AU). We are not sensitive to a possible inner disk with the radius of < 0.21 AU (Espaillat et al. 2010) because it is within the coronagraphic mask.

We examine whether UX Tau C influences the disk geometry of UX Tau A. The Lagrangian point L1 is the point where gravitational forces of the primary and tertiary stars balance each other to a mass point. With the primary mass of $1.3M_{\odot}$, the tertiary mass of $0.16M_{\odot}$ (Kraus & Hillenbrand 2009), and the separation of $2.63''$ (White & Ghez 2001), the location of the point L1 was derived to be $1.9''$ from the primary star. Given that the disk of UX Tau A extends up to $0.8''$, we conclude that the disk is located in the gravitational zone of the primary star and is not gravitationally affected by UX Tau C.

5.2. Polarization models of the circumstellar disk

We construct several polarization models of the circumstellar disk. First, we define the disk geometry. A scattering angle is an angle of deflection from the forward direction of incident light. We consider the disk model based on McCabe et al. (2002). In the disk geometry

of Figure 5, the scattering angle is calculated as

$$\cos(\theta_{\text{scat}} + \phi_{\text{open}}) = \sqrt{1 - \frac{1}{1 + \cos^2(PA - PA_0) \tan^2 i}} (-1)^j, \quad (6)$$

where i is the disk inclination to the line of sight, PA is the position angle measured on the mid-plane of the disk, and PA_0 is the position angle on the near side of the semi-minor axis of the disk. ϕ_{open} is the opening angle of the disk. It expresses the disk height with optical thickness $\tau > 1$. If $\cos PA > 0$, $j = 1$, and if $\cos PA < 0$, $j = 0$ (McCabe et al. 2002). Substituting the inclination, the semi-minor axis, and the height of the disk around UX Tau A into equation (6) allowed us to acquire the scattering angle at each position angle. The disk inclination of 46° was applied. From the semi-major axis of 165° (Figure 1), we assumed that the semi-minor axis direction was 255° .

Next, we consider three scattering approximations. The size parameter for dust grains is defined as $X = 2\pi a/\lambda$. $X = 1$ corresponds to $0.25 \mu\text{m}$ of the grain radius (a) for the H -band observations. We first adopt, as the simplest case, a Rayleigh scattering approximation. The Rayleigh scattering approximation holds in the case of sufficiently small dust grains compared to the observing wavelength ($X \ll 1$). For the H -band observations, it can be applied for the grains with the radii (a) much smaller than $0.25 \mu\text{m}$. The relationship between the degree of polarization and the scattering angle is represented by the following equation (van de Hulst 1957),

$$P = \frac{1 - \cos^2 \theta_{\text{scat}}}{1 + \cos^2 \theta_{\text{scat}}}. \quad (7)$$

The degree of polarization P shows a maximum value P_{max} at $\theta_{\text{scat}} = 90^\circ$ and a minimum value P_{min} at $\theta_{\text{scat}} = 0^\circ$ and 180° . By combining equations (6) and (7), we are able to calculate the polarization pattern on a circumstellar disk.

We consider a geometrically thin disk ($\phi_{\text{open}} = 0^\circ$). It produces a sinusoidal azimuthal profile of the polarization degree (Figure 6). Maximum polarization degrees are $\sim 60\%$ at $PA(P_{\text{max}}) \sim 165^\circ, 345^\circ$. Minimum degrees are $\sim 20\%$ at $PA(P_{\text{min}}) \sim 75^\circ, 255^\circ$. Two P_{max} and two P_{min} have the same values respectively. The interval between $PA(P_{\text{max}})$ and $PA(P_{\text{min}})$ is 90° . Although the data points match the observational polarization degrees quite well for P_{max} , they shows large differences (about 20%) from the observational degrees for P_{min} . The case of a geometrically thick disk with $\phi_{\text{open}} = 30^\circ$ is also shown in Figure 6. Whereas two P_{max} have the same values, two P_{min} have different values. Thus, we conclude that neither disk model matches the observational azimuthal profile of the polarization degrees. Espaillat et al. (2011) suggested that maximum grain size is $10 \mu\text{m}$ at the inner edge of the inner disk and $5 \mu\text{m}$ at the inner edge of the outer disk, from fitting a disk model to the SED of UX Tau A. If the disk consists only of such large dust grains, the Rayleigh scattering approximation is not appropriate for the H -band observations.

Next, we consider a Mie scattering approximation, which is applicable for spherical dust

grains with the size comparable to the observing wavelength ($X \approx 1$, i.e. $a \sim 0.25 \mu\text{m}$). The degree of polarization depends not only on the scattering angle, but also on the grain size, the size distribution, the refraction index, and other grain parameters. Using the observing wavelength, the grain size, the grain size distribution, the refraction index (n), and the absorbing coefficient (k), the Mie scattering program allows us to obtain the degree of polarization as a function of the scattering angle (Figure 7). A similar work done on comet theory using Mie theory, details the procedure (Sen et al. 1991). We found that large dust grains show low P_{max} . In the case that the largest dust grains have a radius as large as 1 mm, the polarization degree shows negative for the large scattering angle (Murakawa 2010). The negative polarization indicates a radial pattern of the polarization vectors. We conclude that any Mie scattering approximation does not reproduce the observed polarizations of UX Tau A. Even if we use a geometrically thick disk, the models are hardly different from that of a geometrically thin disk.

Finally, we focused on geometric optics. It is applicable for interpreting light scattering by irregular shaped particles sufficiently larger than the observing wavelength ($X \gg 1$, i.e. $a \gg 0.25 \mu\text{m}$). We adopted computer simulation results of Grynko & Shkuratov (2003), in which light scattering is calculated for various grains. We used the polarization profiles for 100 faceted particles. Grynko & Shkuratov (2003) calculated it with the refractive indices of some silicate ($n = 1.5$, $k = 0.004$), and $a \sim 30 \mu\text{m}$. We considered that the 100 faceted particles presumably correspond not to the dust grains with smooth spheres but to those with rugged surfaces. The degree of polarization shows 0 % at $\theta_{\text{scat}} = 0^\circ$, 180° and maximum value at $\theta_{\text{scat}} \sim 85^\circ$. These distribution of the polarization degree resembles that of the Rayleigh scattering approximation. One characteristic is that the degree of polarization falls down to about 10 % at $\theta_{\text{scat}} \sim 45^\circ$ and 135° , whereas that in the Rayleigh scattering approximation has about 30 % at $\theta_{\text{scat}} = 45^\circ$ and 135° . With this distribution of the polarization degrees, we constructed the polarization model of a geometrically thin disk (Figure 8). Maximum polarization degrees are $\sim 80\%$ at $PA(P_{\text{max}}) = 165^\circ$ and 335° . Minimum degrees are $\sim 3\%$ at $PA(P_{\text{min}}) = 55^\circ - 85^\circ$ and $225^\circ - 275^\circ$. Although the model shows maximum degrees about 10 % larger than the observed maximum degree at $PA \sim 165^\circ$, it reproduces well the observed minimum polarization degree. Moreover, $PA(P_{\text{max}})$ and $PA(P_{\text{min}})$ of the model are consistent with those of the observed PA s. We did not obtain such a profile in the Mie scattering approximation by spherical grains with $a = 30 \mu\text{m}$. Therefore, we suggest that dust particles in the disk are nonspherical grain with $60 \mu\text{m}$ diameter at 40 AU from the central star. This argument is consistent with no $10 \mu\text{m}$ silicate emission in the UX Tau A spectra, indicating a lack of small dust grains (Espaillat et al. 2010).

We also considered a geometrically thick disk. Assuming vertical hydrostatic equilibrium and no turbulence in the disk, the density profile of the disk is given by

$$\rho(Z) = \rho_0 \exp\left(-\frac{Z^2}{H^2}\right), \quad (8)$$

where H is the scale height and ρ_0 is the density at the disk mid-plane. Muto (2011) indicates

that the disk thickness Z with $\tau = 1$ corresponds to $3H$ for such a disk. The large opening angle of the circumstellar disk, ϕ_{open} , corresponds to large ratio of the scale height to the disk radius (H/R). We simulated thick disks with various ϕ_{open} values. A disk with large ϕ_{open} value shows large interval of $PA(P_{\text{max}})$. For example for the disk with H/R of 0.1, $PA(P_{\text{max}})$ results in 150° and 350° . Moreover, minimum polarization degrees at $PA(P_{\text{min}}) = 70^\circ$ and 250° have different values. It is distinctly different from the polarization profile of UX Tau A. If $\phi_{\text{open}} < 11^\circ$, corresponding to $H/R < 0.067$, the models are consistent with the polarization profile of UX Tau A. We conclude that the geometrical thickness of the UX Tau A disk agrees with $H/R = 0 - 0.067$. Most of the dust grains in the disk have therefore settled into the mid-plane and formed the flat disk. Andrews et al. (2011) found a disk geometry favoring a rather flat disk structure.

The polarization degrees decrease with the semi-major axes (Figure 4). Since the Keplerian velocity is small in the outer part of the disk, it is generally considered that the dust particles in the outer disk have small relative velocities. We consider a slow growth rate of such dust, thus resulting in small dust grains in the outer part of the disk. However, the low polarization degrees in the outer part of the disk are not reproduced by the Rayleigh scattering approximation. The computer simulations of light scattering with geometric optics approximation (Grynko & Shkuratov 2003) calculated the polarization degree profile for grains with various number of facets. They indicated that the maximum polarization degree decreases with decreasing the facet number. We expect dust grains with rough surface in the outer part of the circumstellar disk. Most previous studies of scattered light images from circumstellar disks could explain the scattering (or polarization) function with small, ISM-like grains. For AB Aur, for instance, Perrin et al. (2009) found a similar P_{max} as in this present study, but they could explain the results with more or less typical, small ISM grains. Only recently, Quanz et al. (2011) found some indications based on PDI data, that on the surface of the HD100546 disk micron sized grains might be present. Andrews et al. (2011) used also a rather ISM-like dust population to explain both their interferometric observations and the SED of UX Tau A. However very small P_{min} observed in this work can be reproduced by the scattering model of the dust grains with rough surfaces. To obtain further information of shapes and sizes of the grains, geometric optics models are to be investigated with various parameters.

5.3. *Dust growth in the circumstellar disk*

The forces acting on dust grains in a protoplanetary disk are gas drag force and gravitational force of the central star. In a condition with a temperature typically expected in a circumstellar disk, grains with the sizes less than a few tens micrometers are marginally affected by gas drag forces and dominated by Brownian thermal motion (Weidenschilling 2000). As a consequence of frequent collision and coagulation, the dust grains grow larger. We examine how large dusts can grow during settling into the mid-plane at 40 AU from the central star.

It is claimed that the dust grains grow to several centimeters at 1 AU, during sedimentation (Nakagawa et al. 1981). We calculated the radii of grains settling toward the mid-plane according to the equations for dust growth during sedimentation (Takeuchi et al. 2009). We assumed the dust sticking probability $C = 1$ and the grain bulk density of 1 g cm^{-3} . We do not consider any turbulence in the disk. As a result, we found that the dust grains can grow up to $100 \mu\text{m}$ radius during sedimentation at 40 AU from the central star. Therefore, it is possible for dust grains to grow to $30 \mu\text{m}$ radius at 40 AU from the central star.

Next we evaluate the timescale that the dust grains grow from $0.1 \mu\text{m}$ to $100 \mu\text{m}$ during sedimentation toward the disk plane. We take account of the gas drag. If the circumstellar disk of UX Tau A is optically thin at sub-millimeter wavelengths, the sub-millimeter observations (Andrews et al. 2011) indicate that the gas surface density of the UX Tau A disk at 40 AU from the central star is $\sim 10 \text{ g cm}^{-2}$. For the disk with $H/R = 0.067$, the disk thickness with $\tau = 1$ is about 16 AU at the disk radius of 40 AU. We obtain the average gas density of $4.2 \times 10^{-14} \text{ g cm}^{-3}$ ($2.5 \times 10^{10} \text{ atom cm}^{-3}$). With the relationship between the gas density and the mean free path of gas molecules (Takeuchi et al. 2009), we derive $4.8 \times 10^4 \text{ cm}$ for the gas mean free path. Since the radii of the dust grains up to $100 \mu\text{m}$ is sufficiently smaller than the gas mean free path, the dust grains grow under the Epstein regime. As a consequence of calculating the equation for the sedimentation timescale (Takeuchi et al. 2009), it is revealed that it takes at least 10^5 years for dust grains with $0.1 \mu\text{m}$ radii to settle and grow up to $100 \mu\text{m}$ in radius. The age of UX Tau A is estimated to be about 10^6 years (Kraus & Hillenbrand 2009). We claim that the coagulated growing dusts have already settled into the equatorial plane of the circumstellar disk. It is consistent with our observational evidence that the circumstellar disk of UX Tau A is geometrically thin.

Dust grains with sizes between a few micrometer and a hundred micrometer are entrained by gas toward the central star. Adachi et al. (1976) investigated the spiral motion of the dust grains in a protoplanetary disk. The decay time of the spiral motion corresponds to the infall timescale of the dust grains toward the central star. Applying their calculations, with the radially constant gas density of $4.2 \times 10^{-14} \text{ g cm}^{-3}$, we derived 2×10^6 years for the dust grains with radii of $100 \mu\text{m}$ to infall from 40 AU to the central star. We therefore suggest that the circumstellar disk of UX Tau A still contains such large dust grains.

6. Conclusions

With HiCIAO/AO188 mounted on the Subaru Telescope, we carried out H -band polarimetric imaging observations of UX Tau A, which has been classified as a pre-transitional disk object. The observation revealed a circumstellar disk around UX Tau A at the spatial resolution of $0.1''$ beyond 23 AU from the central star. The disk extends to 120 AU in radius. The disk is inclined by $46^\circ \pm 2^\circ$ as the west side is near. We did not detect evidences of the inner disk and the gap-like structure.

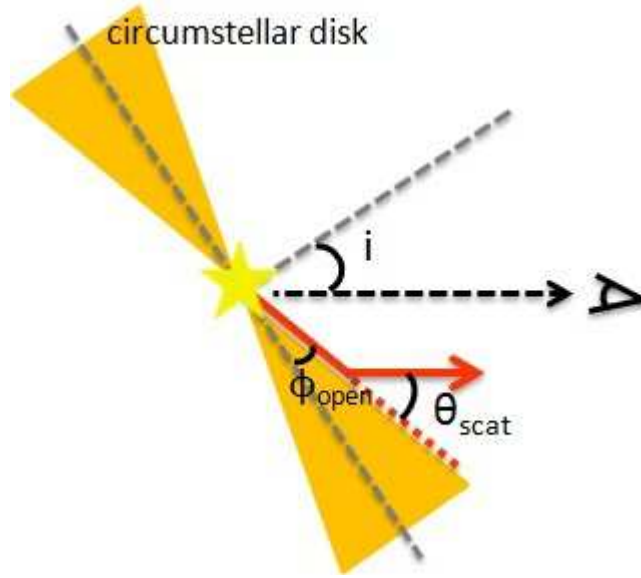


Fig. 5. Schematic view of the disk geometry.

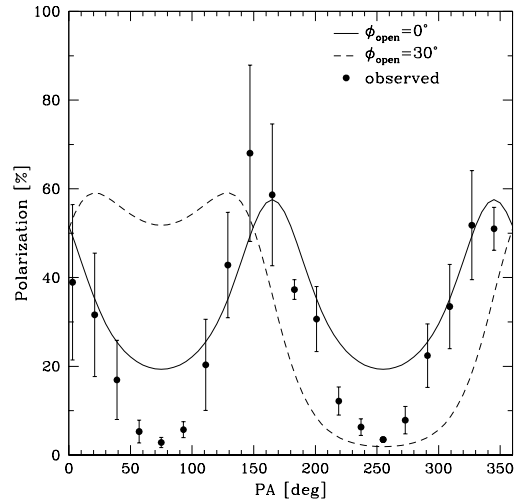


Fig. 6. Azimuthal profiles of the polarization degree. The filled circles show the observed degrees of polarization measured along the ellipse with an eccentricity of 0.72 and a semi-major axis of $0.30''$. The solid line represents the polarization degree of a geometrically thin disk model ($\phi_{\text{open}} = 0^\circ$) and the dashed line shows that of a geometrically thick disk model of $\phi_{\text{open}} = 30^\circ$. We used the Rayleigh scattering approximation. The polarization profiles of the models are convolved with a 20° window in order to match the spatial resolution of the 9×9 pixels binned profile of the observational polarization.

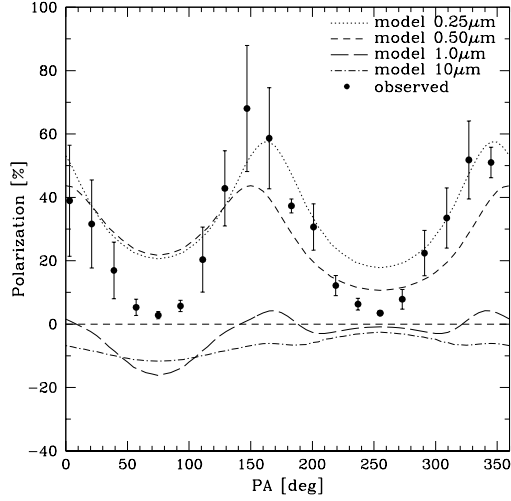


Fig. 7. Azimuthal profiles of the polarization degree. The filled circles show the observed degrees of polarization measured along the ellipse with an eccentricity of 0.72 and a semi-major axis of $0.30''$. We constructed four geometrically thin disk models with the maximum grain radius of 0.25, 0.50, 1.0, and $10 \mu\text{m}$, using the Mie scattering approximation. The polarization profile of each model is shown by the dot, the short dashed, the long dashed, the dashed dotted lines, respectively. We used $0.005 \mu\text{m}$ for the minimum grain radius and $N(a) \propto a^{-3.5}$ for the grain size distribution. The polarization profiles of the models are convolved with a 20° window in order to match the spatial resolution of the 9×9 pixels binned profile of the observational polarization.

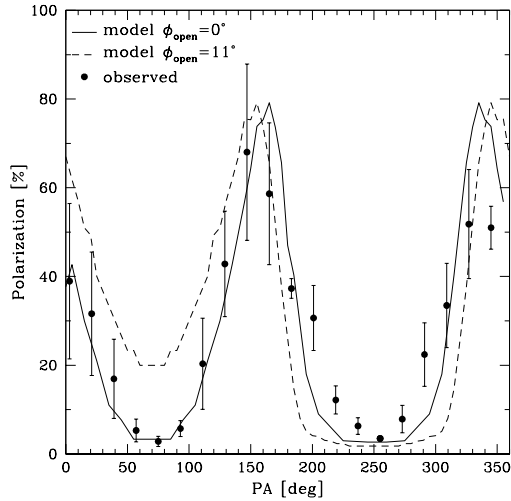


Fig. 8. Azimuthal profiles of the polarization degrees of the circumstellar disk. The filled circles show the observed degrees of polarization measured along the ellipse with an eccentricity of 0.72 and a semi-major axis of $0.30''$. We showed two disk models constructed by the geometric optics approximation. The solid line represents the geometrically thin disk model. The dashed line shows the geometrically thick disk model with $\phi_{\text{open}} = 11^\circ$. The polarization profiles of the models are convolved with a 20° window. Both models approximately reproduce the observed polarization degrees.

The notable feature of the circumstellar disk is the huge variation of the polarization degrees. It varies from 1.6 to 66 %. We constructed several polarization models of the circumstellar disk based on the Rayleigh scattering and Mie scattering approximations. However neither models were consistent with the observational azimuthal profile of the polarization degrees. Focusing on geometric optics, we built the polarization model of the geometrically thin disk with nonspherical grains with the radii of 30 μm . The model reproduced well the observational azimuthal profile of the polarization degree. We suggest that UX Tau A has a geometrically thin disk containing the nonspherical dust grains with the radii of 30 μm .

Such a disk with nonspherical large dust grains is consistent with the core accretion model of planetary formation process. At 40 AU from UX Tau A, the dust grains can grow up to 100 μm in radius by collisional coagulation and settle toward the mid-plane with the timescale of 10^5 years at the earliest. Observational evidence of large dust grains as well as the gap structure in the circumstellar disk provides robust signatures of planetary formation process in the UX Tau A system.

We thank the telescope staff members and operators at the Subaru Telescope. This work is partly supported by the JSPS-DST collaboration. E.L.T. gratefully acknowledges support from a Princeton University Global Collaborative Research Fund grant and the World Premier International Research Center Initiative (WPI Initiative), MEXT, Japan. J. Carson gratefully acknowledges support from NSF grant AST-1009203.

References

- Adachi, I., Hayashi, C., Nakazawa, K. 1976, *Progress of Theoretical Physics*, 56, 1756
Apai, D., Pascucci, I., Brandner, W., et al. 2004, *A&A*, 415, 617
Andrews, S. M., Wilner, D. J., Espaillat, C., Hughes, M., et al. 2011, *ApJ*, 732, 42
Boss, A. P. 1998, *ApJ*, 503, 923
Calvet, N., D'Alessio, P., Hartmann, L., et al. 2002, *ApJ*, 568, 1008
Calvet, N., D'Alessio, P., Watson, D. M., et al. 2005, *ApJ*, 630, 185
Correia, S., Zinnecker, H., Ratzka, Th., Sterzik, M. F. 2006, *A&A*, 459, 909
Elias, J. H. 1978, *ApJ*, 224, 857
Espaillat, C., Calvet, N., D'Alessio, P., et al. 2007, *ApJ*, 670, 135
Espaillat, C., D'Alessio, P., Herna'ndez, et al. 2010, *ApJ*, 717, 441
Espaillat, C., Furlan, E., D'Alessio, P., et al. 2011, *ApJ*, 728, 49
Grynko, Y., Shkuratov, Y. 2003, *Journal of Quantitative Spectroscopy & Radiative Transfer*, 78, 319
Hashimoto, J., Tamura, M., Muto, T., et al. 2011, *ApJ*, 729, 17
Hayano, Y., Takami, H., Oya, S., et al. 2010, *Proc. SPIE*, 7736, 21
Hinkley, Sasha., Oppenheimer, Ben R., Soummer, Re'mi., et al. 2009, *ApJ*, 701, 804
Jones, B. F., Herbig, G. H.. 1979, *AJ*, 84, 1872
Joos, Franco.,; Buenzli, E.,; Schmid, H. M., et al. 2008, *Proc. SPIE*, 7016, 48

Kokubo, E., Ida, S. 1998, *Icarus*, 131, 171
Kokubo, E., Ida, S. 2000, *Icarus*, 143, 15
Kraus, A. L., Hillenbrand, L. A. 2009, *ApJ*, 704, 531
Lucas, P. W., Fukagawa, M., Tamura, M. 2004, *MNRAS*, 352, 1374
McCabe, C., Duchêne, G., Ghez, A. M. 2002, *ApJ*, 575, 974
Murakawa, K. 2010, *A&A*, 518, 63
Muto, T. 2011, *ApJ*, 739, 10
Nakagawa, Y., Nakazawa, K., Hayashi, C. 1981, *Icarus*, 45, 517
Nakagawa, Y., Hayashi, C., Nakazawa, K. 1983, *Icarus*, 54, 361
Nakagawa, Y., Sekiya, M., Hayashi, C. 1986, *Icarus*, 67, 375
Oppenheimer, B. R., Brenner, D., Hinkley, S., et al. 2008, *ApJ*, 679, 1574
Perrin, M. D., Schneider, G., Duchene, G., et al. 2009, *ApJ*, 707, 132
Quanz, S. P., Schmid, H. M., Geissler, K., et al. 2011, *ApJ*, 738, 23
Quanz, S. P., Birkmann, S. M., Apai, D., et al. 2012, *A&A*, 538, 92
Sen, A. K., Deshpande, M. R., Joshi, U. C., et al. 1991, *A&A*, 242, 496
Serkowski, K., Mathewson, D. S., Ford, V. L. 1975, *ApJ*, 196, 261
Silber, J., Gledhill, T., Duchêne, G., Ménard, F. 2000, *ApJ*, 536, L89
Takeuchi, T. 2009, in *Small Bodies in Planetary Systems*, ed. Mann, I., Nakamura, A. M., and Mukai, T. (Springer, Berlin) page1-30
Tamura, M., Hodapp, K., Takami, H., et al. 2006, *Proc. SPIE*, 6269, 28
Tamura, M. 2009, *American Institute of Physics Conference Series*, 1158, 11
van de Hulst, H. C. 1957, *Light Scattering by Small Particles*(New York: John Wiley&Sons)
Weidenschilling, S. J. 2000, *Space Sci. Rev.*, 92, 295
White, R. J., Ghez, A. M. 2001, *ApJ*, 556, 265
Williams, Jonathan P., Cieza, Lucas A. 2011, *ARA&A*, 49, 67